Photoemission from ultrathin metallic films: Quantum size effect, electron scattering, and film structure

M. Jałochowski
Institute of Physics, Maria Curie-Skłodowska University, Pl.M.Curie-Skłodowskiej 1, PL-20-031 Lublin, Poland

H. Knoppe, G. Lilienkamp, and E. Bauer
Physikalisches Institut, Technische Universität Clausthal, D-3392 Clausthal-Zellerfeld, Federal Republic of Germany
(Received 9 March 1992)

The quantum-size-effect structure of ultrathin Pb and Pb-In alloy films on Si(111) surfaces is studied by photoemission spectroscopy in the thickness range from 0 to about 30 monolayers and analyzed, taking into account electron scattering and film structure, which is characterized by high-energy-reflection-electron diffraction.

I. INTRODUCTION

While quantum size effects (QSE's) in semiconductors have long moved from fundamental studies into applications, much less progress has been made in metals since the electron tunneling experiments of Jaklevic *et al.*[1] into thin Pb, Ag, Au, and Mg films. Various other experimental techniques have been used subsequently in QSE studies with metal films such as resistivity or low-energy electron transmission measurements (for references see Ref. 2) but only recently has ultraviolet photoelectron spectroscopy (UPS) been shown to be particularly well suited for the determination of quantum size energy levels in thin films. The UPS studies of Ag films on Si(111),[3] Au(111),[4,5] Cu(111),[6] and of Na, Ba,[7] and Cs (Ref. 8) films on Cu(111) have significantly advanced our understanding of QSE's in thin films but there are still many open questions in the interpretation of the experimental results: the influence of the photoelectron transport processes following photoexcitation, of imperfections in the volume and on the surface of the film, and of the simplifying assumption of an electron in a simple rectangular potential well, to name only a few, which will be among those addressed in the present study.

Inelastic, quasielastic, and elastic scattering change energy and/or momentum of the photoexcited electron so that it escapes from the film with a different energy and/or momentum and is not detected at the final energy $E_f=\hbar\omega-E_i$ corresponding to the initial QSE state E_i and the incident photon energy $\hbar\omega$. Imperfections such as point defects (e.g., impurities) in the volume or line defects (steps) on the surface determine to a large extent quasielastic and elastic scattering. The thickness fluctuations have a much more profound influence: they cause locally varying QSE conditions and thus smear out the QSE features. Therefore, for an understanding of the intensity and sharpness of QSE features, the thickness distribution has to be properly characterized. Finally, the energy of QSE levels is not accurately described by the simple quantum-well model as calculations for Al(111) layers show.[9] This has to be taken into account in the quantitative discussion of the QSE energies.

In order to shed some light on the questions discussed above, the electronic structure of ultrathin pure Pb and of Pb-In alloy layers on Si(111) surfaces was studied by UPS and their growth and microstructure were monitored by reflection-high-energy-electron diffraction (RHEED), in particular by RHEED specular beam intensity oscillations. This system was chosen because it was well characterized in earlier studies and found to be well suited for QSE studies because of its approximate monolayer-by-monolayer growth at low temperatures.[2,10] Indium was added to Pb in order to vary the impurity concentration over a wide range. This is possible with In because (i) Pb and In form solid solutions over a wide composition range with only small changes of the lattice constant a_0 with concentration $C[\Delta a_0/(a_0\Delta C)\simeq 3.7\times10^{-4}$/at. % In] and (ii) because the surface energies of the two metals are very similar ($\gamma_{Pb}=0.61$, $\gamma_{In}=0.67$ J/m^2) so that there is little tendency towards surface or interface segregation of one of the components.

II. EXPERIMENT

The experiments were performed in a VG-ESCALAB photoelectron spectrometer to which a molecular-beam epitaxy (MBE) chamber equipped with RHEED, a mass spectrometer, and quartz-crystal oscillator were attached. A liquid-nitrogen-trapped diffusion pump and titanium sublimators produced a base pressure of 4×10^{-9} Pa.

The substrates were Si(111) crystals with about 1000 Ω cm resistivity at room temperature and typical dimensions $18\times4\times1$ mm^3. After chemical etching in a 19:1 mixture of HNO_3 and HF, rinsing in distilled water and methanol the final surface cleaning was performed in the vacuum system before deposition by flashing for a few seconds to about 1450 K, which produced a clean Si(111) surface as indicated by a sharp Si(111)-(7×7) RHEED

pattern without SiC contamination.

Deposition of about one monolayer (ML) of Au followed by 3 min annealing at 950 K and for 3 min at 600 K produced the (6×6)Au superstructure on the Si surface. Direct resistive heating of the Si crystal was used. The substrate could be cooled to 110 K by making thermal contact between the rotatable holder and a liquid-N_2 container.

The quartz-crystal monitor was calibrated by resistivity measurements[2] during Pb-film deposition. The growth mode and the structure of the films were monitored by RHEED. The beam energy was usually 15 keV and a Faraday cup was used to measure the intensity oscillations of the specularly reflected electron beam.

For photoelectron spectroscopy we used the He I line (21.22 eV) from a Leybold cold cathode capillary discharge lamp with a homebuilt triple-reflection polarizer,[11] which gave a linear polarization of 90%. The spectra were recorded with an energy resolution of better than 150 and 100 meV for measurements with and without polarizer. An aperture at the entrance of the analyzer input lens reduced the acceptance to a cone with 1° half angle. The angle between incident light and detected electrons was always 36°. The position of sharp and isolated peaks could be reproduced to within ±50 meV. An additional error of 30 meV had to be taken into account for the uncertainty in the determination of the Fermi level position. Thus the absolute binding energies E_B are accurate to within ±60 meV.

Pb was evaporated from a Mo crucible at rates ≤0.05 ML/min during the UPS measurements and 1 ML/min during the RHEED studies. In could be evaporated simultaneously from another Mo crucible. The ratio [Pb]:[In] in the film was determined by rate calibration with the quartz-crystal monitor.

The photoelectron intensity measurements were done in two modes. In the first mode the energy distribution of photoelectrons emitted in the direction normal to the film surface was measured at fixed coverages over a broad energy range corresponding to binding energies E_B from 0 to 9 eV. These measurements give an overview of the evolution of the UPS features of the ultrathin films from those of the substrate. In the second mode the photoelectron intensity was measured continuously during deposition while the energy of the analyzer was scanned from E_B=0.07 to 1.37 eV in steps of 0.1 eV/(10 s). This method of data collection allowed us, after further computer evaluation, to obtain plots of the photoelectron intensity I versus thickness d of the thin film. Typically about 200 scans were recorded in this mode during the growth of a 30-ML-thick film.

III. RESULTS

A. RHEED intensity oscillations and RHEED patterns

The thickness dependence of the specular beam intensity is shown in Fig. 1 for Pb and Pb-In alloy films on the Si(111)-(6×6)Au surface at 110 K. For pure Pb a strong damping of the RHEED intensity oscillations was seen whereas for the Pb-In alloy more than 100 periods of oscillations could be observed easily. At about 30 at. % of In they were best developed. In the initial stage of growth which is dominated by film-substrate interaction the oscillations become increasingly irregular with increasing In content. Above 4 ML, however, the reverse

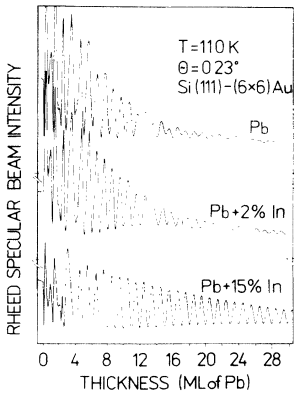

FIG. 1. RHEED specular beam intensity oscillations during the growth of Pb and In-Pb alloy films on a Si(111)-(6×6)Au surface at 110 K, [$\bar{1}$12] azimuth, glancing angle 0.23°.

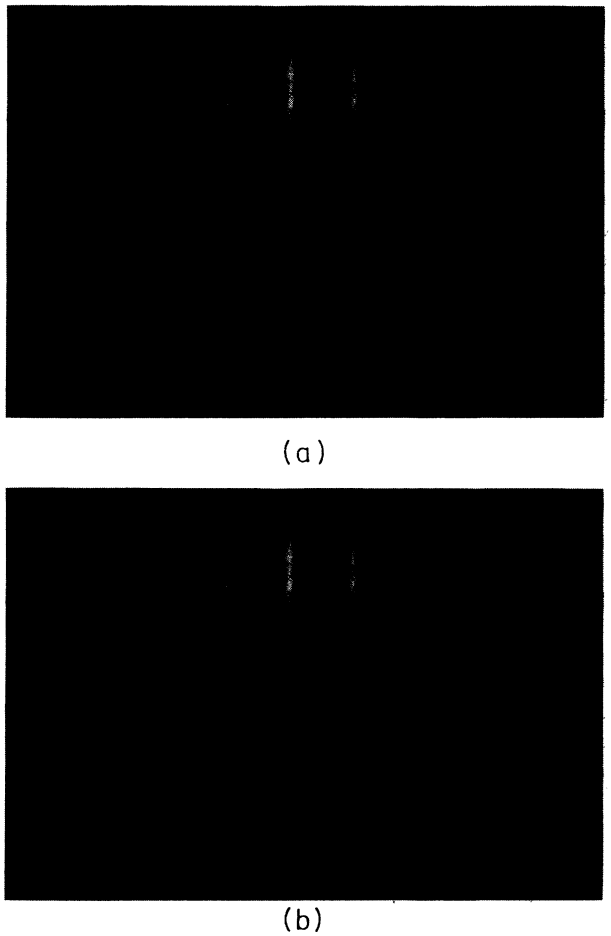

FIG. 2. RHEED patterns from (a) a 30-ML-thick pure Pb film and (b) a 30-ML-thick Pb–25 at. % In film. Si(111)-(6×6)Au substrate at 110 K, [$\bar{1}$10] azimuth and glancing angle 0.95°.

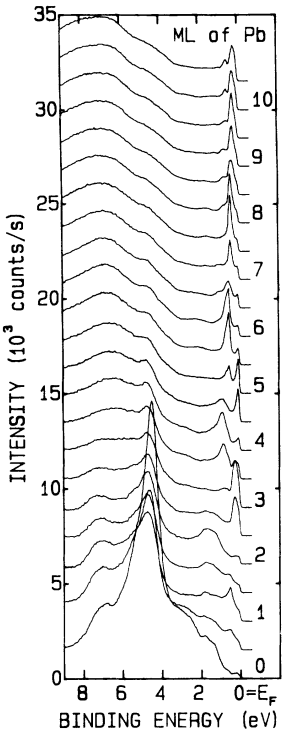

FIG. 3. Angular resolved photoemission spectra of Pb films on Si(111)-(6×6)Au at 110 K. The spectra were taken with unpolarized He I light at normal emission. The parameter is the film thickness in ML units.

is true: the modulation superimposed on the monolayer oscillations which is seen clearly in the pure layer decreases with increasing In content.

The RHEED pattern from a 30-ML-thick pure Pb film [Fig. 2(a)] showed streaks with superimposed three-dimensional features. For a Pb–25 at. % In film [Fig. 2(b)] the streaks are smooth with no visible spots. Both patterns were taken in the Si[$\bar{1}$10] azimuth at a glancing angle of incidence of $\Theta = 0.95°$ at 110 K. Pure Pb films on Si(111)-(6×6)Au have the orientation Si(111)‖Pb(111), Si[$\bar{1}$10]‖Pb[11$\bar{2}$] whereas in Pb–25 at. % In films an admixture of Si[$\bar{1}$10]‖Pb [$\bar{1}$10] is seen. The full widths at half maximum (FWHM's) of the RHEED streaks, after subtraction of the instrumental broadening, were identical in both cases, 0.04 $Å^{-1}$(±10%), corresponding to an average terrace size of about 25 Å.

B. Photoemission

Results of the measurements in the first mode are shown in Fig. 3 for pure Pb layers. The spectra are taken at 110 K at normal emission with unpolarized He I light. The first spectrum is from the clean substrate and is dominated by the Au 5*d* peak 4.4 eV below the Fermi level. This peak rapidly decreases with Pb coverage and the features characteristic of the Pb layers, in particular near E_F, develop.

Figure 4 presents results from measurements taken in the second mode. The data show the dependence of the photoelectron intensity I upon thickness d for Pb, Pb–10 at. % In, and Pb–30 at. % In films at fixed binding energy. In this manner the details of the coverage dependence are seen much better.

IV. THEORY

A. Quantum-well states

Unfortunately, until now there is no theoretical study of the band structure of Pb crystals consisting of only a few monatomic layers. Therefore, in order to calculate the QSE energy levels, we use the model of the finite-potential quantum well with parameters determined ex-

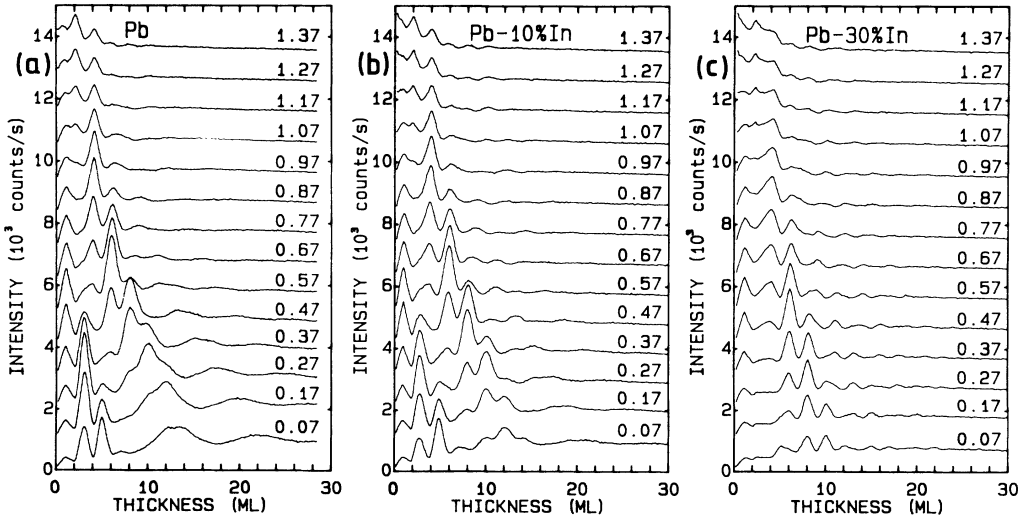

FIG. 4. Photoemission intensities of (a) Pb, (b) Pb–10 at. % In, and (c) Pb–30 at. % In films as a function of thickness. The parameter is the binding energy E_B in eV.

perimentally by Anderson and Gold[12] and Jaklevic and Lambe.[1] In our model the ultrathin Pb film consists of n monatomic layers with a thickness of $d_0=2.8435$ Å at 110 K. The bulk lattice constant at 4 K (4.915 Å) and the data of Ref. 12 are used to obtain the Fermi wave number $k_F=1.596$ Å^{-1} along ΓL ($\langle 111\rangle$) in the extended Brillouin zone scheme. From Ref. 1(b) (Table I and Fig. 11 therein) we find the effective mass $m^*=1.002m_0$. Thus near E_F the $E(k_\perp)$ relation can be best fitted by the equation $E(k_\perp)=-U_0+\hbar^2k_\perp^2/(2m^*)$ with $U_0=9.685$ eV. The work function ϕ of Pb(111), which is needed to determine the depth $U_0+\phi$ of the potential well, is taken as 4.35 eV.[13]

Simple calculations for the finite-potential quantum well[14] with these parameters give the sets of energy levels shown in Fig. 5 and are compared in this figure with the $E_B(d)$ values of the observed photoemission intensity maxima. The dots denote the calculated values whereas the open squares are the experimental data. The thin lines connect some of the levels with the same quantum number $N(N=5,10,\ldots,40)$.

For the finite potential well $k_\perp$ is given by the equation $k_\perp=(N-\Delta)\pi/(nd_0)$, $N=1,2,3,\ldots$, $n=1,2,3,\ldots$. Δ is a measure for the penetration of the wave function into the region outside of the potential well of width nd_0.

For the infinite potential well ($\Delta=0$) this relation can be written as $N\lambda/2=nd_0$. In thick films $k_\perp=1.596$ Å^{-1} at E_F, i.e., $\lambda_F=3.937$ Å. Therefore matching of the QSE wave function to the well width for energies near E_F and for $\Delta=0$ occurs approximately for $n/N\simeq\lambda_F/(2d_0)=0.692\simeq\frac{2}{3}$, that is, for $N=3,6,9,\ldots$ and for $n=2,4,6,\ldots$ independent of the number of monolayers n.

In the finite-potential well the ratio N/n is replaced by the thickness-dependent ratio $(N-\Delta)/n$. In Fig. 5 the QSE states with $N/n=\frac{3}{2}$ (or $2N-3n=0$) are connected by the thick line labeled with $i=0$ while the lines labeled by $i=-1$, $+1$, 2, and 3 are drawn through the calculated families of QSE states satisfying the condition $2N-3n=i$, respectively, that is, the condition $N\lambda/2=[(2N-i)/3]d_0$.

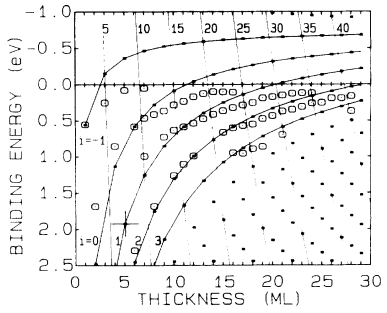

FIG. 5. Theoretical (dots) and experimental (open squares) data of the QSE levels in thin Pb(111) films as a function of the film thickness in steps of 1 ML. The theoretical data are obtained from the model of the one-dimensional finite depth quantum well (see text). The experimental data are taken from Figs. 3 and 4(a). The thin lines connect some of the levels with the same quantum number N ($N=5,10,\ldots,40$). The other lines connect the QSE state families with $i=-1$, 0, 1, 2, and 3 (see text). The large cross marks a state occurring also in Fig. 9.

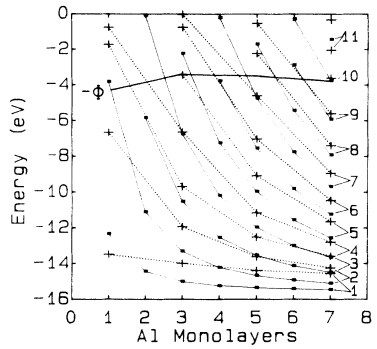

FIG. 6. Comparison of the theoretical subband energies in Al(111) from self-consistent-field pseudopotential calculations (crosses) (only for 1, 3, 5, and 7 ML) (Ref. 9) and from the model of the finite depth quantum well (dots) for Al(111) (see text). The Fermi level calculated in Ref. 9 is denoted by $-\phi$. The zero of energy is the vacuum level in this figure.

Because of lack of detailed calculations of the quantization of the Pb electronic states upon lowering the dimensionality in the $\langle 111\rangle$ direction it is not possible to discuss rigorously the positions of the QSE levels. In order to check the applicability of the simplified quantum-well model we compare the results obtained by Batra *et al.*[9] from full self-consistent-field pseudopotential calculations of thin Al(111) slabs with the results obtained for the finite-potential well model for Al(111). Figure 6 shows the results of Ref. 9 (Fig. 13 therein) and results of our calculations with parameters $d_0=2.34$ Å, $k_F=1.756$ Å^{-1}, $m^*=1.0375m_0$, $U_0=11.33$ eV,[15] and work function $\phi=4.24$ eV.[16] The dots connected with full lines represent the energies of the QSE levels obtained from the finite-potential well model whereas the crosses are the subband energies at the $\bar{\Gamma}$ point calculated by Batra *et al.* for 1, 3, 5, and 7 ML, only.[9]

It is evident from this figure that there are only a few (n,N) pairs for which the results of the two calculations coincide. In general and in particular at 1 ML the deviations between them are much larger than the deviations of the experimental from the theoretical data for Pb in Fig. 5. For 5 and 7 ML near E_F ($E=-\phi$) the quantum numbers N (given in Fig. 6 on the right) of neighboring dots and crosses are identical; but obviously the finite depth quantum-well model is insufficient to predict the precise energy values of the QSE levels. Therefore we concentrate our attention on the intensities and their thickness dependence.

B. Photoexcitation in quantum wells

We restrict our discussion to normal-emission spectra, neglecting possible emissions from the substrate and interfaces on both sides of the ultrathin film (no "surface photoemission"). We first consider the energy bands in the ΓL direction ($\langle 111\rangle$) of bulk Pb in order to determine the transitions possible with $\hbar\omega=21.22$ eV. Using UPS, Horn *et al.*[17] have performed an extensive experi-

mental and theoretical study of bulk Pb. They placed the bottom of the s-like band (10 ± 0.5) eV below the Fermi level and determined accurately the p-like band shape in the vicinity of the Fermi level. Figure 7 summarizes their theoretical and experimental results and shows also the direct electronic transition for He I excitation. It is obvious that without relaxation of the rule of momentum conservation perpendicular to the (111) surface occupied states at E_F are not accessible to an UPS experiment with $\hbar\omega < 21.9$ eV. In the following we discuss the possible causes leading to the relaxation of the momentum conservation rule.

According to Shung and Mahan[18] the expression for the current emitted per unit solid angle and unit energy normal to the surface can be reduced to a one-dimensional integral:

$$\frac{d^2I}{d\Omega dE} = \frac{em_0}{2\pi^2}\int_0^{k_\perp} dk_{i\perp} p\,|M(p,k_{i\perp})|^2 \times\delta(E-E_i(k_{i\perp})-\hbar\omega+\phi)\,, \quad (1)$$

where $E_i(k_{i\perp})$ is the initial-state energy, and $E=p^2/2m_0$ is the kinetic energy of the emitted electron in vacuum. $M(p,k_{i\perp})$ is the excitation matrix element; the δ function ensures energy conservation. The results of the exact calculations of the matrix element are given in Ref. 19. For constant photoelectron energy as plotted in Fig. 4, we can assume that the matrix element is a constant multiplied by a function $F(\Delta k_\perp)$ to account for the limited periodicity normal to the surface which has several causes: (i) the limited penetration of the photon field, (ii) the finite inelastic mean free path L of the photoelectrons, (iii) the finite elastic mean free path due to scattering of the photoelectrons by impurities, (iv) the surface relaxation and, most importantly (v) the small thickness of the film. Mahan[19] has calculated this function for the half space considering causes (i) and (ii). It is easy to calculate this function for a finite thickness nd_0 which yields

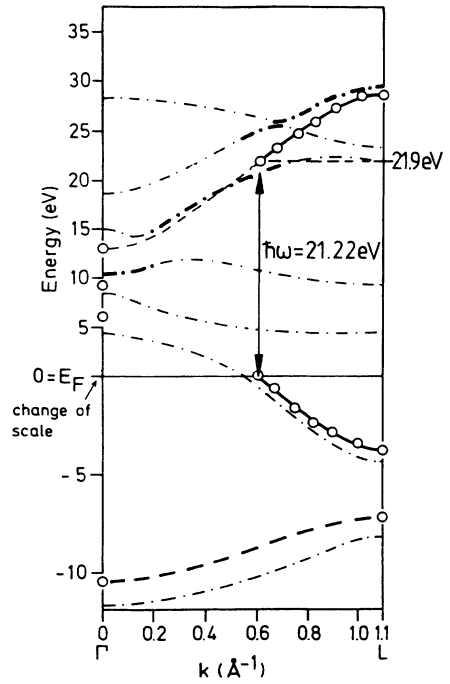

FIG. 7. The band structure along ΓL of bulk Pb (Ref. 17). Circles denote the experimentally derived values. Dot-dashed lines indicate calculated bands (enhanced in the regions in which they are close to the free-electron-like parabolas). The arrow indicates the direct transition for He I excitation.

$$F(\Delta k_\perp) = \frac{[1-\exp(-2nd_0/L)]^2+4\exp(-2nd_0/L)\sin^2(\Delta k_\perp nd_0/2)}{[1-\exp(-2d_0/L)]^2+4\exp(-2d_0/L)\sin^2(\Delta k_\perp d_0/2)}\,. \quad (2)$$

Cause (iii) can be included by reducing L by an amount proportional to the density of scattering centers, $\Delta k_\perp$ gives the relaxation of the conservation rule for the normal component of the momentum. The calculated function $F(\Delta k_\perp)$ for the photoelectron inelastic mean free path in our experiment, $L=6$ Å, is shown in Fig. 8 for several thicknesses nd_0. With increasing L this function strongly peaks at $\Delta k_\perp=0$ and finally, for $L\to\infty$, has the shape of the δ function. For a given film thickness it varies only slightly (about 20%) in the energy range of our interest.

Figure 9 shows as an example the $k_\perp$ relaxations required for observing the occupied quantum states in a 5-ML-thick film. The state closest to E_F ($N=7$) is marked by a cross in Fig. 5. The final-state band $E_3(k_\perp)$ is approximated by a straight line in the $k_\perp$ range of interest, except for small $k_\perp$ values at which the calculated band structure (see Fig. 7) is assumed. It is seen that the states below $N=5$ (at 5 ML) are invisible because they are not accessible with He I radiation.

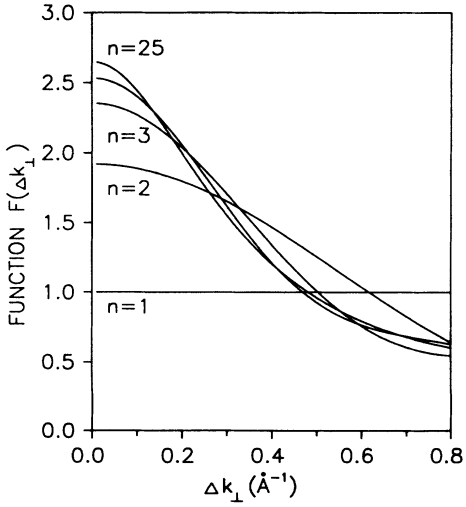

FIG. 8. Function $F(\Delta k_\perp)$ calculated according to Eq. (2) for finite film thicknesses nd_0 ($n=1$, 2, 3, 4, and 25 ML) and for the photoelectron inelastic mean free path $L=6$ Å.

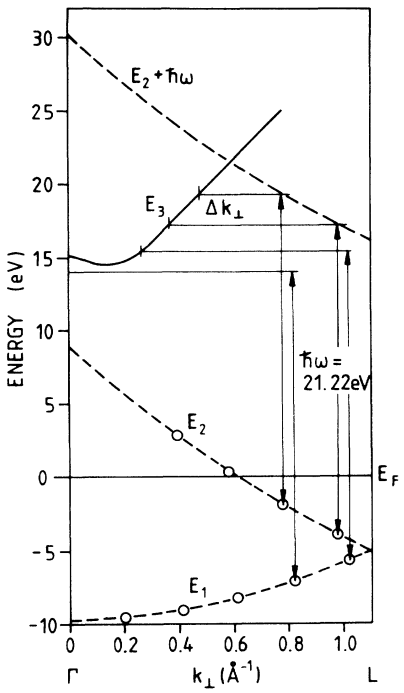

FIG. 9. The band structure of a 5-ML-thick Pb film. Marked on the bands E_1 and E_2 are the discrete states calculated with the finite depth potential well model (see text). $E_3(k_\perp)$ (approximated by a straight line in the $k_\perp$ range of interest) is taken from Ref. 17. Arrows indicate the possible direct transitions with He I radiation with relaxation of the $k_\perp$ conservation rule.

At fixed $d\Omega$ and analyzer energy E_A we obtain from (1) the measured photoemission intensity:

$$I(nd_0,E_A)\propto\int_0^\infty dE\,B(E_A,E)E^{1/2}\times\sum_{k_{iN\perp}}F(\Delta k_{N\perp})\delta(E-E_i(k_{iN\perp},nd_0)-\hbar\omega+\phi)\ . \quad (3)$$

$E_i(k_{iN\perp},nd_0)$ is the calculated QSE energy-level matrix indicated by the dots in Fig. 5. The factor $B(E_A,E)$ accounts for smearing effects such as the finite resolution of the energy analyzer or the broadening of the QSE levels arising from the finite temperature and from crystal imperfections. A Gauss distribution function with $\sigma=0.2$ eV was used in the calculations.

C. Photoemission from quantum wells

We assume that the penetration of the light is sufficiently large so that the electric field is uniform in the whole sample. The rate of photoelectron excitation is then proportional to the electron density. For photoemission normal to the surface of the sample this density per unit area of the surface is given by the square of the one-dimensional QSE wave function

$$\Psi_{N,n}(z)=(2/nd_0)^{1/2}\sin(N\pi z/nd_0)\ .$$

The excited photoelectrons have an inelastic mean free path L and only a fraction of the total number of photoelectrons leaves the thin film without energy loss. The probability of finding a photoelectron, which was excited from QSE level N in the quantum well, outside of the thin film is thus

$$P(N,nd_0)=\int_0^{nd_0}\exp(-z/L)|\Psi_{N,n}(z)|^2dz\ . \quad (4)$$

Neglecting the phase shift Δ we have $k_\perp=N\pi/(nd_0)$, and in the energy range near the Fermi level in which most of the data were collected (Figs. 4 and 5) $k_\perp\simeq k_F$ and $N\simeq k_F nd_0/\pi$ so that $\Psi_{N,n}(z)=(2/nd_0)^{1/2}\sin(2\pi z/\lambda_F)$ and the integral (4) can be easily calculated. The result of the calculation of Eq. (4) for $L=6$ Å $\simeq 2d_0$, 10 Å $\simeq 3.5d_0$, and 20 Å $\simeq 7d_0$ is shown in Fig. 10.

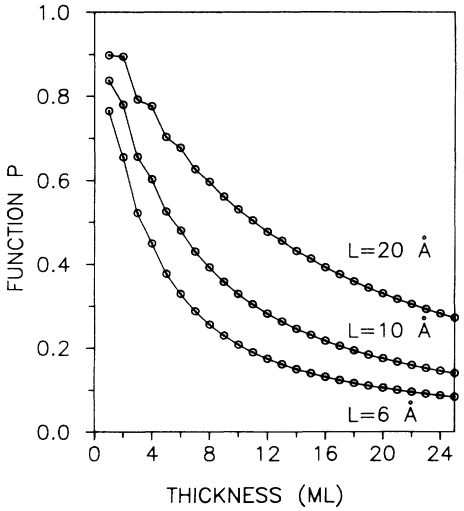

FIG. 10. Probability of finding an excited photoelectron without inelastic scattering as a function of the film thickness. Parameter is the inelastic mean free path L.

QSE photoelectrons may also not be detected in the normal-emission geometry used here because of having been scattered elastically out of the normal direction by crystal imperfections such as impurities, for example, In, or surface steps. As mentioned before, possible scattering by In can be taken into account by a concentration-dependent reduction of the mean free path. In order to obtain the decrease in normal photoemission intensity at large N and large E_B seen in Fig. 4 with increasing In concentration L had to be decreased from 6 Å to 5 and 4 Å for 10% and 30% In, respectively.

D. The influence of the surface roughness

In this section we take into account the fact that the width of the quantum well varies locally at fixed mean thickness as a consequence of the nature of the growth of the epitaxial film. The measurements of the RHEED oscillations indicate that Pb grows initially monolayer by monolayer. This mode of growth can be greatly prolonged by coevaporation of In (Fig. 1).

Depending on the film thickness the number of monolayers involved in the formation of the growth front changes from 2 ML for perfect monolayer-by-monolayer

growth to 3 or more ML for less perfect growth.

For a thin film growing with the growth rate $1/\tau$ [ML/s] the mean film thickness d is

$$d(t)=\sum_{n=1}^{\infty}\Theta_n(t)d_0 \ , \tag{5}$$

where $\Theta_n(t)$ is the layer coverage of the nth level. To determine $\Theta_n(t)$ we use the "distributed growth model" given in Ref. 20. This model takes into account the lateral structure in the plane of the film by distributing adatoms among the monolayers according to the number of "reactive" sites available. Of the $[\Theta_n(t)-\Theta_{n+1}(t)]/\tau$ atoms per unit time arriving on top of the nth layer, a fraction α_n transfers to the nth layer and a fraction $(1-\alpha)$ remains in the $(n+1)$th layer. The time-dependent coverage is given by the equation

$$\frac{d\Theta_n}{dt}=\alpha_n\frac{\Theta_n-\Theta_{n+1}}{\tau}+(1-\alpha_{n-1})\frac{\Theta_{n-1}-\Theta_n}{\tau} \tag{6}$$

and

$$\alpha_n=A\frac{c_n(\Theta)_n}{c_n(\Theta_n)+c_{n+1}(\Theta_{n+1})} \ .$$

A is a phenomenological parameter that measures the net rate of transfer from one layer to the next. c_n is an effective perimeter for the capture of an adatom to a given layer. We choose the dependence $c_n(\Theta)=\Theta_n(1-\Theta_n)^{1/2}$ which corresponds to a growth model in which both the number and the size of two-dimensional clusters and islands change during film growth.[20] The coverage $\Theta_n(t)$ at time t is given by the solution of the set of coupled differential equations (6) subject to the initial conditions $\Theta_0(t)=1$ and $\Theta_n(0)=0$ for $n\geq 1$.

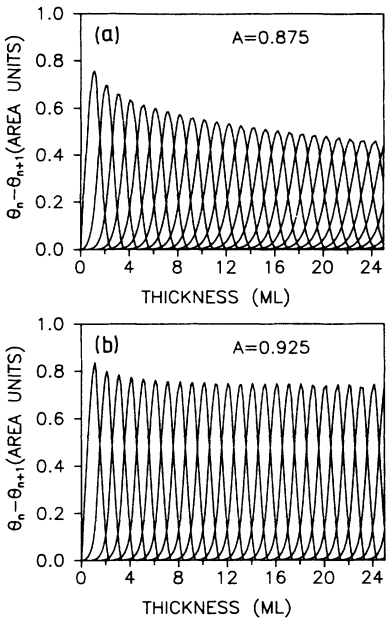

FIG. 11. Solution of Eq. (6) with (a) $A=0.875$ and (b) $A=0.925$ (see text).

The solutions of Eq. (6) with $A=0.875$ and 0.925 are shown in Fig. 11. It is seen that more than 2 ML are involved in the film growth for films thicker than 1 ML. Consequently the photoemitted current consists of contributions from regions with different thicknesses nd_0 and area fractions $\Theta_n-\Theta_{n+1}$. The final expression for the photoemission intensity is therefore

$$I(d,E_A)\propto\sum_{n=1}^{\infty}P(nd_0)(\Theta_n-\Theta_{n+1})\int_0^{\infty}dE\,B(E_A,E)E^{1/2}\sum_{k_{iN\perp}}F(\Delta k_{N\perp})\delta(E-E_i(k_{iN\perp},nd_0)-\hbar\omega+\phi) \ . \tag{7}$$

Figure 12 shows the results of the evaluation of Eq. (7) for the calculated QSE levels of Fig. 5 with $L=6$ and 4 Å for $A=0.875$ and 0.925.

V. DISCUSSION AND SUMMARY

This work has shown that QSE energy levels in ultrathin Pb and Pb-In alloy films down to 1-ML thickness can be detected by measuring photoemission spectra during film growth.

The simple finite-potential quantum-well model was used to calculate the QSE levels in films with different thicknesses. Several causes altering the photoemission were taken into account in a calculation of the thickness dependence of the intensity: (i) the relaxation of the conservation rule of the perpendicular momentum caused by the finite film thickness and by the limited photoelectron mean free path L, (ii) the thickness dependence of the spatial density distribution of the electrons in the initial state and the damping of the outgoing photoelectrons, and (iii) the discrete nature of the film thickness governed by the growth mode of the thin film.

The finite-potential quantum-well model gave qualitative agreement between the experimental and the theoretical data of the QSE. In order to check the applicability of the simple quantum-well model its predictions for Al(111) layers were compared with the exact calculations by Batra *et al.*[9] From this comparison it was evident that the quantum-well model does not describe properly the location of the QSE levels. Nevertheless, this model was sufficient to explain the general behavior of the QSE phenomena in photoemission from the ultrathin epitaxial films studied here.

This work stressed the importance of the relaxation of the conservation rule of $k_\perp$ in thin films and its impact on photoelectron excitation when direct transitions are forbidden.

The most serious influence is that of the growth mode of the film. The discrete nature of the film thickness variation (with increment of d_0) assures that the peaks are

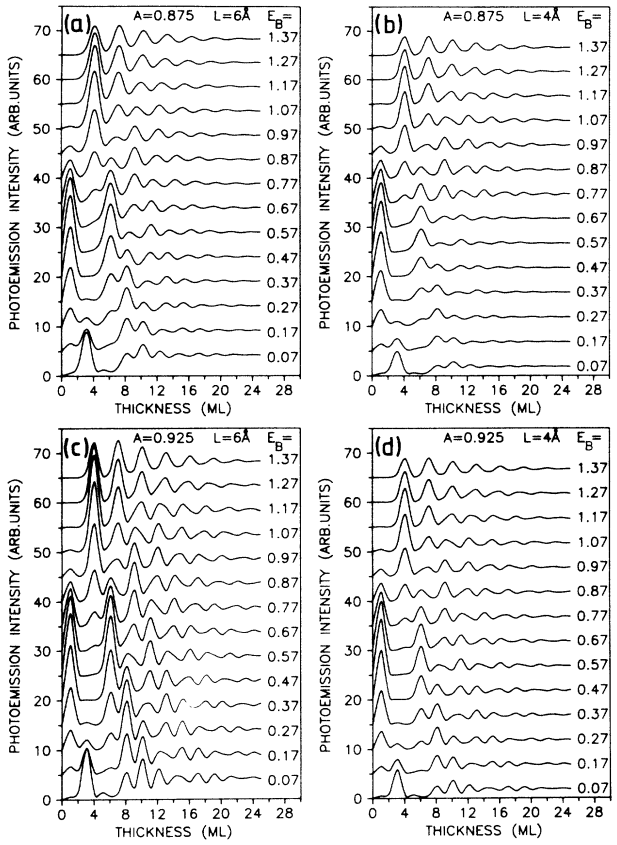

FIG. 12. Calculated photoemission intensity as a function of the average Pb film thickness d according to Eq. (7) for $A=0.875$ and 0.925 with mean free path $L=6$ and 4 Å. The parameter is the binding energy E_B in eV.

centered at integer numbers of monolayers. In the vicinity of E_F the peaks were well resolved with a separation of 2 ML, at least for the first 10 ML. This separation was predicted by the finite-potential well model (Fig. 5) in which the calculated QSE levels belonging to one of the families (for example with $i=1$) appear every 2 ML. Due to the smearing of the energy levels and the finite resolution of the electron analyzer neighboring levels could be detected even at the same E_B.

For larger E_B, where the slope of the lines denoted with $i=1$, 2, and 3 is much larger than near E_F, the QSE levels belonging to neighboring branches i, $i+1$ occur every 3 ML (see Fig. 5). This 3-ML periodicity was weakly visible in the initial stage of the film growth [Fig. 4(c)] and clearly in the calculated curves of Fig. 12 for large E_B. For small E_B and a wider thickness range the periodicity oscillates between 2 and 3 ML which causes the strong modulation of the QSE peaks seen in the measurements and in the calculations. According to Fig. 12 (0.07 eV) the maxima of this modulation should be expected for 3, 10, and 19 ML of Pb. This is close to the experimental data of Fig. 4(a) where for $E_B=0.07$ eV the highest photoelectron intensity was measured for 5, 13, and 22 ML.

As it is seen from the calculated curves of Figs. 12(a) and 12(c), the change in the growth mode leading to the simultaneous growth of 5 ML (5-ML growth front with $A=0.875$) smears out the QSE structures but does not change the average photoelectron intensity. The decrease of the mean free path L from 6 to 4 Å preserves the QSE structures but damps the average intensity [Figs. 12(a) and 12(b)]. Thus we could deduce that in the experimental data for pure Pb [Fig. 4(a)] less perfect growth occurs with larger L whereas for Pb–10 at. % In and Pb–30 at. % In [Figs. 4(b) and 4(c)] the growth is more perfect but L is smaller. In the former case the average photoelectron intensity is larger and the QSE features are smeared out. This was visible especially for the curves with $E_B=0.07$ eV for large d. In the latter case the average intensity was smaller but the 2-ML periodicity extended to larger thicknesses.

The weakness of the QSE features for Pb–30 at. % In films thinner than about 4 ML was caused by the structural transition clearly visible in the RHEED measurements and mentioned in Sec. III A.

In conclusion, we showed that a proper analysis of the photoemission from ultrathin size-quantized films requires discussion of many parameters describing the thin film. Even without the knowledge of the exact band structure of thin Pb(111) films, qualitative agreement between the calculated and experimental data was achieved; a more detailed analysis can be made as soon as exact calculations of the band structure of thin Pb(111) films are available.

ACKNOWLEDGMENTS

This work was supported in part by the Volkswagen Foundation (Hannover, Germany), in part by the Deutsche Forschungsgemeinschaft, and in part by Grant No. 2-0382-91-01 of the Polish Committee of Scientific Research.

[1](a) R. C. Jaklevic, J. Lambe, M. Mikkor, and W. C. Vassel, Phys. Rev. Lett. **26**, 88 (1971); (b) R. C. Jaklevic and J. Lambe, Phys. Rev. B **12**, 4146 (1975).

[2]J. Jałochowski and E. Bauer, Phys. Rev. B **38**, 5272 (1988).

[3]A. L. Wachs, A. P. Shapiro, T. C. Hsieh, and T.-C. Chiang, Phys. Rev. B **33**, 1460 (1986).

[4]T. Miller, A. Samsavar, G. E. Franklin, and T.-C. Chiang, Phys. Rev. Lett. **61**, 1404 (1988).

[5]S. Å. Lindgren and L. Walldén, J. Phys. Condens. Matter **1**, 2151 (1989).

[6]M. A. Mueller, A. Samsavar, T. Miller, and T.-C. Chiang, Phys. Rev. B **40**, 5845 (1989); M. A. Mueller, T. Miller, and T.-C. Chiang, *ibid.* **41**, 5214 (1990).

[7]S. Å. Lindgren and L. Walldén, Phys. Rev. Lett. **59**, 3003 (1987).

[8]S. Å. Lindgren and L. Walldén, Phys. Rev. Lett. **61**, 2894 (1988); Phys. Rev. B **38**, 3060 (1988).

[9]I. P. Batra, S. Ciraci, G. P. Srivastava, J. S. Nelson, and C. Y. Fong, Phys. Rev. B **34**, 8246 (1986).

[10]M. Jałochowski and E. Bauer, J. Appl. Phys. **63**, 4501 (1988);

Surf. Sci. **213**, 556 (1989).
[11]K. Jacobi, P. Geng, and W. Ranke, J. Phys. E **11**, 982 (1978).
[12]J. R. Anderson and A. V. Gold, Phys. Rev. **139**, A1459 (1965).
[13]M. Tikhov and E. Bauer, Surf. Sci. **203**, 423 (1988).
[14]R. M. Eisberg, *Fundamentals of Modern Physics* (Wiley, New York, 1961).
[15]A. M. Radwan and M. Taut, Phys. Status Solidi B **76**, 605 (1976).
[16]J. K. Grepstad, P. O. Gartland, and B. J. Slagsvold, Surf. Sci. **57**, 348 (1976).
[17]K. Horn, B. Reihl, A. Zartner, D. E. Eastman, K. Hermann, and J. Noffke, Phys. Rev. B **30**, 1711 (1984).
[18]Kenneth W.-K. Shung and G. D. Mahan, Phys. Rev. B **38**, 3856 (1988).
[19]G. M. Mahan, Phys. Rev. B **2**, 4334 (1970).
[20]P. I. Cohen, G. S. Petrich, P. R. Pukite, G. J. Whaley, and A. S. Arrott, Surf. Sci. **216**, 222 (1989).

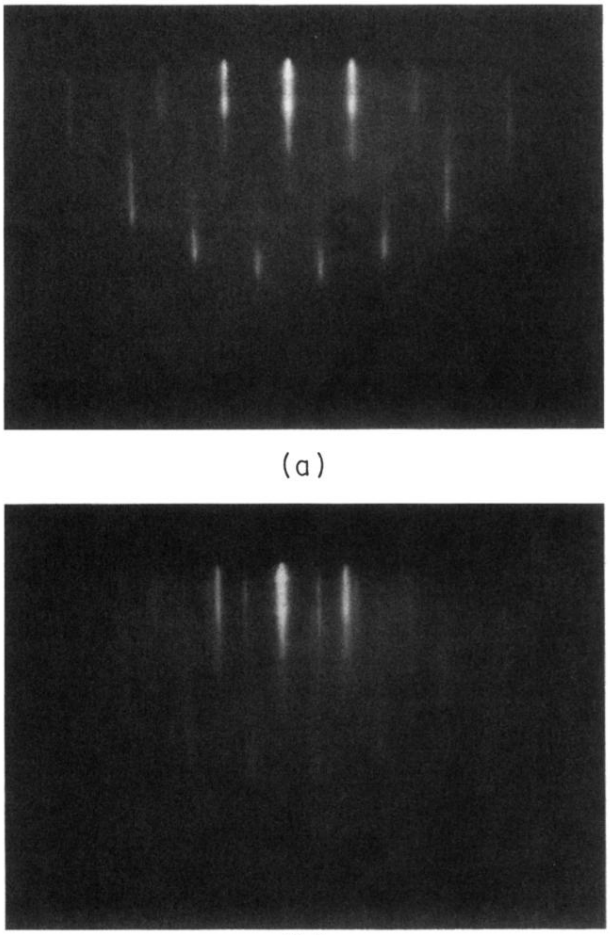

FIG. 2. RHEED patterns from (a) a 30-ML-thick pure Pb film and (b) a 30-ML-thick Pb–25 at. % In film. Si(111)-(6×6)Au substrate at 110 K, [$\bar{1}$10] azimuth and glancing angle 0.95°.